Taylor & Francis
Taylor & Francis Group

Artificial Cells, Nanomedicine, and Biotechnology
An International Journal

ISSN: 2169-1401 (Print) 2169-141X (Online) Journal homepage: informahealthcare.com/journals/ianb20

Sageretia thea (Osbeck.) modulated biosynthesis of NiO nanoparticles and their *in vitro* pharmacognostic, antioxidant and cytotoxic potential

Ali Talha Khalil, Muhammad Ovais, Ikram Ullah, Muhammad Ali, Zabta Khan Shinwari, Dilawar Hassan & Malik Maaza

To cite this article: Ali Talha Khalil, Muhammad Ovais, Ikram Ullah, Muhammad Ali, Zabta Khan Shinwari, Dilawar Hassan & Malik Maaza (2018) *Sageretia thea* (Osbeck.) modulated biosynthesis of NiO nanoparticles and their *in vitro* pharmacognostic, antioxidant and cytotoxic potential, Artificial Cells, Nanomedicine, and Biotechnology, 46:4, 838-852, DOI: 10.1080/21691401.2017.1345928

To link to this article: https://doi.org/10.1080/21691401.2017.1345928

Published online: 07 Jul 2017.

ARTIFICIAL CELLS, NANOMEDICINE, AND BIOTECHNOLOGY, 2018
VOL. 46, NO. 4, 838–852
https://doi.org/10.1080/21691401.2017.1345928

Sageretia thea (Osbeck.) modulated biosynthesis of NiO nanoparticles and their *in vitro* pharmacognostic, antioxidant and cytotoxic potential

Ali Talha Khalil[a,b,c], Muhammad Ovais[a], Ikram Ullah[a], Muhammad Ali[a], Zabta Khan Shinwari[a,d], Dilawar Hassan[b,c] and Malik Maaza[b,c]

[a]Department of Biotechnology, Quaid-i-Azam University, Islamabad, Pakistan; [b]Nanosciences African Network (NANOAFNET), iThemba LABS-National Research Foundation Somerset West, Western Cape, South Africa; [c]UNESCO-UNISA Africa chair in Nanoscience and Nanotechnology, College of Graduate Studies, University of South Africa, Pretoria, South Africa; [d]Pakistan Academy of Sciences, Islamabad, Pakistan

ABSTRACT

NiO nanoparticles are biosynthesized using *Sageretia thea* (Osbeck.) aqueous leave extracts and their biological activities are reported. Nanoparticles (~18 nm) were characterized through XRD, ATR-FTIR, EDS, SAED, HR-SEM/TEM and Raman spectroscopy. Antibacterial activity was investigated against six pathogenic bacterial strains (gram positive and gram negative) and their corresponding minimum inhibitory concentrations (MICs) were calculated. UV-exposed nanoparticles were investigated to have reduced MICs relative to the NiO nanoparticles have not been exposed to UV. Moderate linear fungal growth inhibition was observed while *Mucor racemosus* (percentage inhibition 64% ± 2.30) was found to be most susceptible. Cytotoxicity was confirmed using brine shrimps lethality assay (IC_{50} 42.60 μg/ml). MTT cytotoxicity was performed against *Leishmania tropica*-KWH23 promastigotes and amastigotes revealed significant percentage inhibition across the applied concentrations. IC_{50} values were calculated as 24.13 μg/ml and 26.74 μg/ml for the promastigote and amastigote cultures of *Leishmania tropica*. NiO nanoparticles were found. Moderate, antioxidant potential was concluded through assays like DPPH, TAP and TAC. Furthermore, protein kinase inhibition and alpha amylase inhibition is also reported.

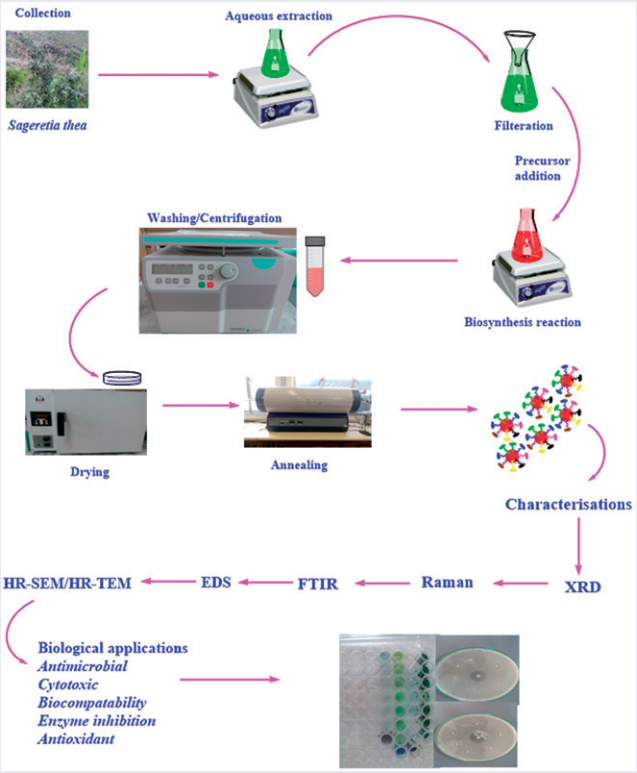

ARTICLE HISTORY
Received 24 April 2017
Revised 11 June 2017
Accepted 19 June 2017

KEYWORDS
Sageretia thea; NiO; cytotoxicity; antimicrobial; antioxidant; antileishmanial

CONTACT Ali Talha Khalil talhakhalil.qau@gmail.com

Introduction

Metallic oxides present a bright area of research because of their interesting physio-chemical, electronic and optical characteristics [1,2]. Therefore, metal oxide nanoparticles like zinc oxide, copper oxide, iron oxide, cobalt oxide, etc. have been frequently synthesized because of their interesting properties for a wide array of applications in electronics, sensors [3], storage devices [4], catalysis [3], drug delivery [5], magnetic resonance imaging [2] and as biomedicine [2]. With the ongoing developments on the interface of nanoscience, metal oxide nanoparticles have gained tremendous popularity for the development of new and effective strategies in biomedicine. Nanoscale matter are different from the microscale counter parts in terms many properties like chemical, mechanical, electro-optical, magneto-optical and surface area to volume ratio which signify them as an effective tool in biomedical applications [6].

Because of its super conductance, chemical stability, electro catalysis, and efficient electron transfer ability, nano-NiO has attracted many researchers [7]. Nano-scaled nickel oxide, presented by a wide band gap (3.7–4.0 eV) is an intrinsic p-type semiconductor [8] used in numerous biological applications. It has been used in adsorption of the toxic pollutants and dyes [9]. Because of their anti-inflammatory nature, they can be used in biomedicine [10]. The cytotoxic effects of nano-NiO have been previously established by the release of ROS and Ni^{++} leading to oxidative damage [11].

Several chemical and physical methods have been proposed for the synthesis of nickel oxide nanoparticles. Co-precipitation, electro deposition, sol-gel chemistry, hydrothermal synthesis, combustion synthesis, solvothermal route, galvanostatic anodization, etc. have been developed to synthesize the NiO nanoparticles [12–16]. However, these synthesis methods are accompanied by some disadvantages that limits their widespread applications [17]. Chemical synthesis routes often generates toxic chemical waste lines while physical means required massive energy input [18,19]. To overcome the problem of toxic wastes and energy imbalance, greener and ecofriendly methods have been proposed [20]. Biological resources, such as plants and microorganisms can be used in a rapid, effective, simple and economical way to produce the desired metal oxide nanoparticles. Green procedures involving medicinal plants are becoming a popular approach for nanoparticle synthesis [21]. Plant extracts are used as capping and reducing agents in green chemistry approach. These plant extracts can act as a biotemplate which controls the size, shape and morphology of the nanoparticles [22].

In this study, a complete green procedure for the synthesis of single phase nano-NiO has been reported by using the aqueous leaf extracts of medicinal plant *Sageretia thea* (Osbeck.). *Sageretia thea* belongs to the rhamnaceae family [23]. The medicinal uses of *S. thea* (Bird Plum/English) are well documented and it is mostly used in the treatment of jaundice, hepatitis, circulatory and cardiovascular disease [23–25]. Biosynthesis of NiO nanoparticles has been successfully demonstrated in recent years and therefore there is a growing interest in NiO nanoparticles synthesis via green route. A general study layout is summarized in Figure 1. Recently, biosynthesis through fungal biomass has been reported [26,27]. Plants like *Moringa oleifera* [2], *Callistemon viminalis* [8], *Nephelium lappaceum* [28], *Agathosma betulina* [17], *Tamarix serotine* [29], etc. have been successfully used for biosynthesis of nano-nickel oxide. Complementing to the limited literature on biomedical applications of bioinspired NiO nanoparticles, a comprehensive study was designed to investigate their pharmacological properties.

Experimental

Plant material processing

The collected plant sample was identified as *S. thea* in the Department of Plant Sciences, QAU, Islamabad, Pakistan. Herbarium specimen (MOSEL-343) was deposited in the herbarium of Molecular Systematics and Applied Ethnobotany Lab (MoSAEL), Department of Biotechnology, QAU. Fresh leaves were rinsed in running distilled water, shade dried and grounded to fine powder in a Willy mill. Grounded plant material was used for aqueous extraction. For extraction of bioactive components from the leaves, 30 g of grounded powder was added to 200 ml deionized water and heated to 80 °C for 1 h on magnetic stirrer hotplate [17]. The resultant solution was filtered thrice to obtain aqueous extracts.

Biosynthesis

Previously established procedure was applied for the biosynthesis of nickel oxide nanoparticles [17]. To the obtained aqueous extracts (pH 5.7), 6.0 g of $NiNO_3$ was added as a precursor salt for the biosynthesis of NiO nanoparticles. Following the addition of precursor, the solution (pH 4.3), was heated up to 60 °C for ~1 h. Following such heating phase, precipitates were observed. The resultant solution was allowed to cool down to room temperature, followed by centrifugation and washing with distill water for 3 times at 1000 rpm/10 min. Obtained precipitate assumed as NiO or $Ni(OH)_2$ was kept for drying at 100 °C for ~2 h. Dried powdered was annealed in a ceramic crucible at 500 °C in open air furnace. Following such phase, the dried nanoparticles underwent extensive dehydration, decomposition and evolution of gases leading to highly crystalline nanoparticles with colour change from brown to greyish.

Characterizations

Various techniques were used for the characterization of annealed nickel oxide nanoparticles. X-ray diffractometer (model Bruker AXS D8 Advance) with irradiation line Kα of copper ($\lambda = 1.5406$ A°) was used to investigate the crystalline nature of the biogenically synthesized nanoparticles. XRD analysis was carried out and their corresponding size was calculated using Scherer equation $\{<\emptyset_{size}> = K\ \lambda/\Delta\theta_{1/2}\ \cos\theta\}$. FTIR spectra were recorded in the range of 400–4000 cm^{-1}. Raman spectrum was recorded from 0 cm^{-1} to 2000 cm^{-1} with a laser line of 473 nm and average excitation power of 2.48 mW. Energy-dispersive X-ray spectroscopy was carried

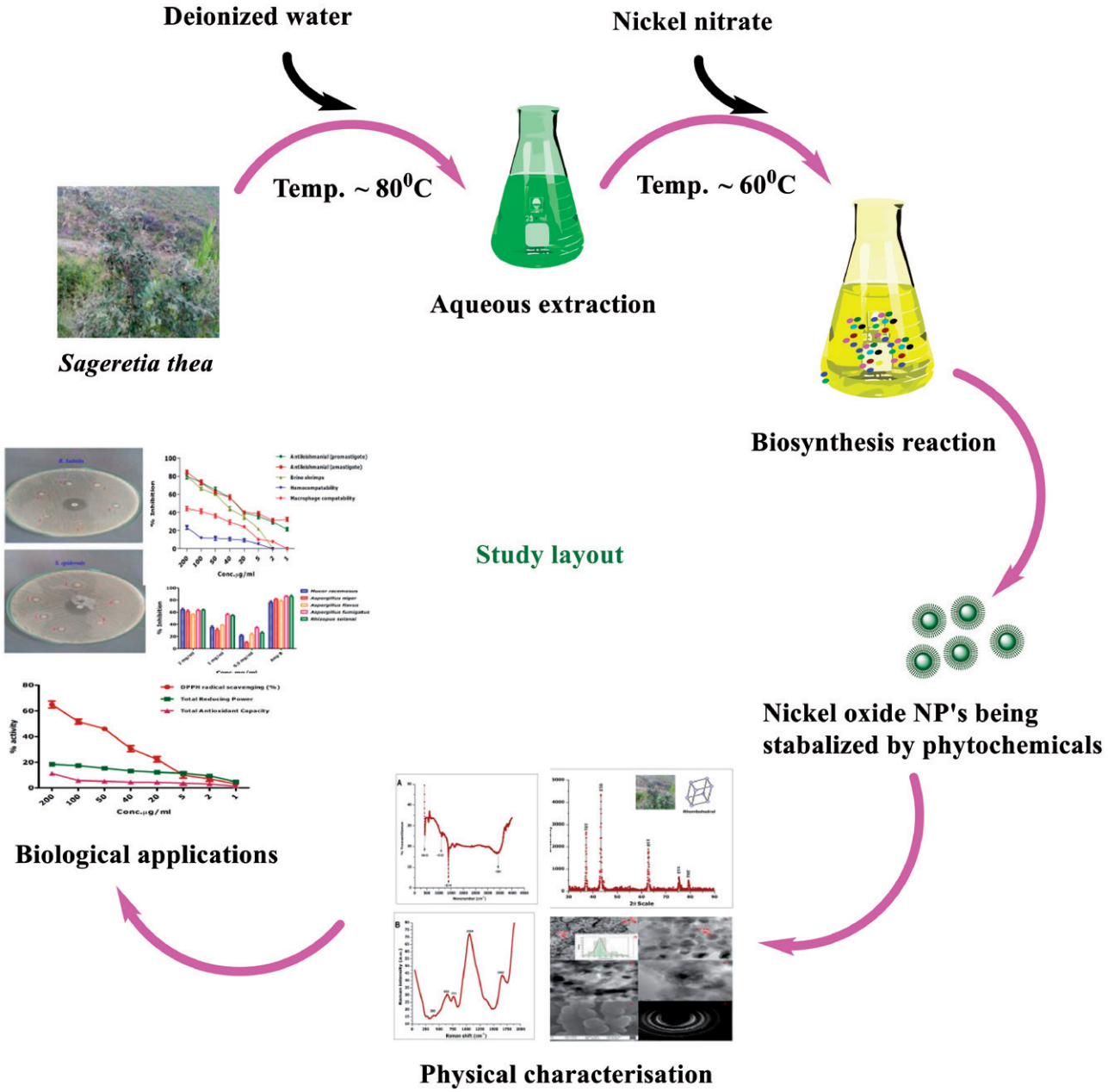

Figure 1. Study design.

out to determine the elemental composition. HR-TEM and HR-SEM were utilized to investigate the particles morphology and size distribution.

Antimicrobial assays

Antibacterial activity

Previously described disc diffusion assay [30] was used to investigate the antibacterial properties of synthesized NiO nanoparticles, whereas their minimum inhibitory concentrations (MICs) were calculated. Already available gram positive and gram negative strains were used. Microbial cultures were refreshed on a Nutrient Agar media (Oxoid-CM0003), then transferred to the nutrient broth and kept in a shaker incubator (Temp: 37 °C; RPM: 200) for growing to the optical density of 0.5 which corresponds to 1×10^8 CFU/ml. 200 µl of standardized culture were used to make uniform microbial lawns. 6 mm filter discs loaded with 10 µl of test sample were carefully placed on the uniform lawns while gentamycin (10 µg) discs were used as positive control. Bacterial plates were incubated for 24 h at 37 °C and inhibition zones were measured across 1000 µg/ml to 31.25 µg/ml. MICs for the bio-inspired NiO nanoparticles were further investigated. Microorganisms investigated are against three gram positive bacterial strains (*B. subtilis* ATCC: 6633, *S. aureus* ATCC: 25923 and *S. epidermis* ATCC: 14990) and three gram negative bacterial strains (*Klebsiella pneumonia* ATCC: 4617, *E. coli* ATCC: 15224 and *Pseudomonas aeruginosa* ATCC: 9721). Considering the debate of UV illumination on the enhancement of the

bactericidal effect, the NiO nanoparticles were illuminated under UV light for 20 min. Germicidal 6 Watt UV Lamp 6GT5 (Sankyo-denki, Hiratsuka, Japan) was used as a source of UV, whereas same method was used to determine the antibacterial efficacy.

Antifungal activity

Linear mycelial growth inhibition assay was used as described previously [31]. Sabouraud Dextrose Liquid medium (Oxoid CMO147) supplemented with 1.5% agar technical (Oxoid LP0012) was used to prepare fungal growth media. 66.6 µl of the test samples were poured to the autoclaved media and allowed for solidification in a slanting position. Fungal spores were inoculated at the based on the slant with nichrome wireloop, and incubated at 37 °C for 48 h. Media devoid of any sample was used as negative control while 250 µg/ml amphotericin B was used as positive control.

Linear mycelial growth inhibition was calculated as:

$$\%\ \text{linear growth inhibition} = 100 - \left[\left\{\frac{\text{Growth in sample (cm)}}{\text{Growth in Negative control (cm)}}\right\} \times 100\right]$$

The antifungal activity was investigated against *Aspergillus niger* (FCBP:0918), *Aspergillus flavus* (FCBP:0064), *Aspergillus fumigatus* (FCBP:66), *Mucor racemosus* (FCBP:0300) and *Rhizoctonia solani* (FCBP:0040).

In vitro *cytotoxicity assays*

Brine shrimp cytotoxicity

To assess the cytotoxic potential of the bioinspired NiO nanoparticles, brine shrimps lethality was carried out as discussed previously using *Artemia salina* larvae in a 96-well culture plates [32,33]. Eggs of *A. salina* (Ocean star, USA) were incubated from 24 h to 48 h under light at 30 °C in sea water (38 g/L supplemented with 6 mg/L dried yeast). Pasteur pipette was used to harvest 10 mature phototrophic nauplii. Test concentrations of bioinspired NiO nanoparticles were applied while dimethyl sulphoxide (DMSO) and doxorubicin were used as positive and negative controls, respectively. Number of the dead shrimps was investigated after 24 h and percentage inhibition was calculated. Median lethal dose (IC_{50}) was calculated using table curve software.

Antileishmanial assay (promastigotes and amastigotes)

MTT cytotoxic assay [33] was performed against promastigote and amastigote cultures of *Leishmania tropica* KWH23. *Leishmania* can exist in 2 forms: promastigotes (outside the human body) and amastigotes (inside the human body). Promastigotes are flagellated while amastigotes are ovoid and non-flagellated [34]. M199 medium added with 10% heat inactivated foetal bovine serum (FBS) was used for culturing parasite. Parasites at the density 1×10^6 cells/ml were used against various concentrations ranging from 200 µg/ml to 1 µg/ml were used. The seeded 96-well plate was kept in 5% CO_2 incubator at 24 °C for 72 h. Amp B was used as positive control. Readings were taken using spectrophotometer and IC_{50} values were calculated using table curve software. Percentage inhibition was calculated as:

$$\%\ \text{Inhibtion} = \left[1 - \left\{\frac{\text{Absorbance of sample}}{\text{Absorbance of Control}}\right\}\right] \times 100$$

Biocompatibility assays

Hemolytic assay

To assess the hemo-compatible nature of the synthesized nanoparticles, hemolytic assay was performed as described previously. Freshly isolated erythrocytes were isolated by centrifugation (14,000 rpm/5 min) of 1 ml fresh blood from the apparently healthy human. Erythrocyte suspension was prepared by adding 200 µl erythrocytes to 9.8 ml phosphate buffer saline (pH 7.2). Erythrocyte suspension (100 µl) was treated with the biogenically synthesized NiO nanoparticles and incubated for 1 h at 35 °C in 96-well plate. Readings were taken at 530 nm to investigate the hemoglobin release. DMSO and Triton X-100 were used as negative and positive controls. Percent hemolysis was investigated as:

$$\%\ \text{Hemolysis} = [AB_S - AB_{NC} \div AB_{PC} - AB_{NC}] \times 100$$

Biocompatibility with macrophages

MTT cytotoxicity against freshly isolated macrophage cells was carried out as described previously [33]. Ficoll–Gastrografin-based method was used for the isolation of macrophages. Blood was diluted with HBSS (Hank's buffered salt solution) which was gently layered on Ficoll–Gastrografin [35]. The resultant was centrifuged at 400 g/30 min, subsequently purified with percoll gradient (density 1.064 g/ml) pre-adjusted with sterilized deionized water. Isolated macrophages were cultured in RPMI medium with 10% FBS, 25 Mm HEPES, streptomycin (0.1 mg/ml) and penicillin 100 U/ml. Culture was incubated in humidified incubator with 5% CO_2 to a density of 1×10^5 cells/well. Growth control, that is, macrophage culture without any addition, was used as positive control. Percentage inhibition was calculated as:

$$\%\ \text{Inhibition} = [1 - \{\text{Sample absorbance} \div \text{Control absorbance}\}] \times 100$$

Enzyme inhibition assays

Protein kinase (PK) inhibition

PK activity was carried out as discussed previously [30]. Uniform lawns of the standardized *Streptomyces* 85E strain were prepared after pre-adjustment of the optical density to 0.5. Autoclaved 6 mm filter disc were placed carefully on microbial lawn and 10 µl of sample was added. Surfactin and DMSO were used as positive and negative controls, respectively. Clear and bald zones were measured.

Alpha amylase inhibition

Previously established protocol was used to investigate the alpha amylase inhibition [33]. Reaction mixture contained

15 µl phosphate-buffered saline (PBS), 25 µl α-amylase enzyme, 10 µl of samples and 40 µl of starch solution which were added stepwise. Reaction mixture with all the ingredients was incubated for 30 min at 50 °C followed by addition of 20 µl (1 M HCL) and 90 µl of iodine solution. Blank solution contained deionized water, starch and PBS while positive and negative controls comprised of acarbose and deionized water, respectively. Enzyme inhibition was calculated as:

$$\%\ \text{Enzyme inhibition} = [\{OD_S - OD_N\} \div \{OD_B - OD_N\}] \times 100$$

whereas "OD_S", "OD_N" and "OD_B" correspond to the optical densities of sample, negative control and blank.

Antioxidant assays

DPPH

DPPH was carried out using standard procedure [33]. Various concentrations ranging from 200 µl to 1 µl were used. 25 ml of methanol was added to 2.4 mg of 2,2-diphenyl 1-picrylhydrazyl (DPPH) to prepare the reagent solution. Ascorbic acid and DMSO were used as positive and negative controls. The electrons in DPPH-free radicals give maximum absorption at 517 nm. Absorption changes when DPPH becomes paired with a cation and form a reduced DPPH. Colour change from deep violet to pale yellow is observed which can be quantified. Readings were recorded at 517 nm. Percent-free radical scavenging was calculated as:

$$\%\ \text{Scavenging} = \left[\left\{1 - \frac{AB_S}{AB_C}\right\}\right] \times 100$$

TAC

TAC was investigated using previously described phosphomolybdenum method procedure [36]. The reagent solution was prepared by adding 0.6 M H_2SO_4, 28 mM NaH_2PO_4 and 4 mM $(NH_4)_6\ Mo_7O_{24}\ 4H_2O$ stepwise followed by incubation at 95 °C for 90 min. Readings were recorded at 695 nm and results were expressed as number of µg equivalents of ascorbic acid per mg of the sample, that is, µg AAE/mg.

TRP

Potassium ferricyanide-based method was used to investigate TRP [37]. 40 µl of test sample was mixed 50 µl of PBS followed by incubation at 50 °C for 20 min. 50 µl of (10%) tri-chloro acetic acid was added to the mixture and 3000 rpm for 10 min. Supernatant (166.6 µl) was added to $FeCl_3$ (33.3 µl) in a 96-well plate. Ascorbic acid and DMSO were used as negative and positive controls and absorbance was recorded at 630 nm. The results were expressed as ascorbic acid equivalents per mg.

Results

Physical characterizations

X-ray diffraction was carried out for the nanomaterial annealed at 500 °C in open air furnace. All the obtained Bragg peaks are corresponding to (101), (012), (110), (113) and (202) are the crystallographic reflections of rhombohedral nickel oxide crystallite with standard lattice parameters $<a> = 0.29$ nm and $<c> = 0.72$ nm, which are consistent with the joint committee on powder diffraction standards (JCPDS) pattern no. 00–044-1159. The face-centred cubic lattice belongs to the space group R-3 m (166). Average size of nickel oxide nanoparticles was calculated as Debye-Scherer equation was employed to calculate the size of average nanoparticles which was found to be ~18 nm. XRD analysis is depicted in Figure 2(A,B). No other associated compounds were found up to the level of XRD, suggesting the pure phase of the biosynthesized nanocrystals. Size distribution, morphology and shape were studied through HR-TEM/HR-SEM (Figure 3, inset). After the digitization of the images using Image-J software, an average size distribution of ~18 nm (Figure 3(A–C)) is revealed which is consistent with the results from XRD. Shape was investigated as spherical while the degree of crystallinity was also confirmed by the SAED pattern as indicated in Figure 3(G). Shape of the nanoparticles was deduced as spherical.

For the detection of any other surface interface-bounded compounds, ATR-FTIR over the spectral range (4000 cm^{-1} to 400 cm^{-1}) was carried out as indicated in Figure 4(A). The strong absorption observed at ~418 cm^{-1} is attributed to the Ni-O vibration in stretching mode [8] while the broad

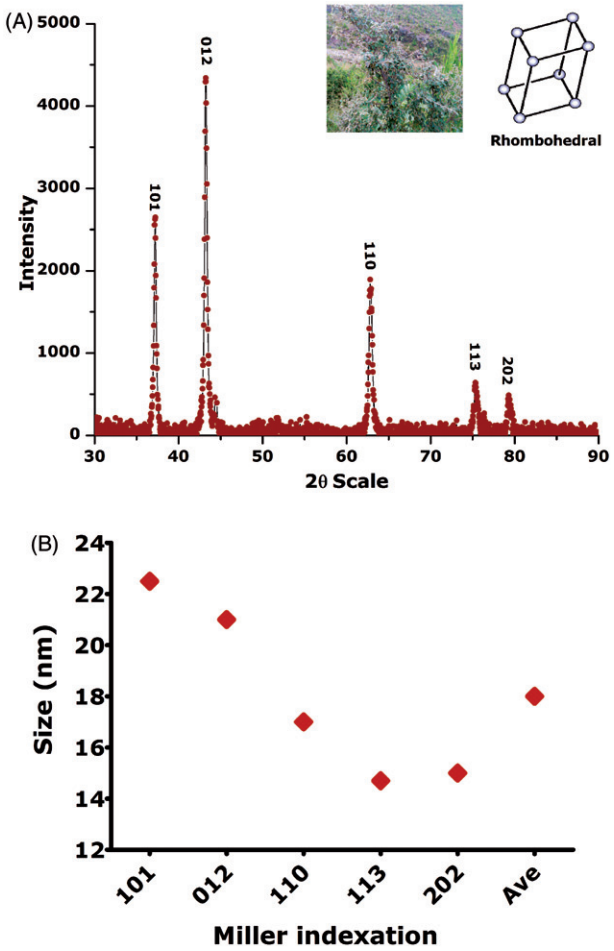

Figure 2. XRD analysis. (A): Typical XRD pattern of NiO annealed at 500 °C; (B): size calculation according to Scherer approximation.

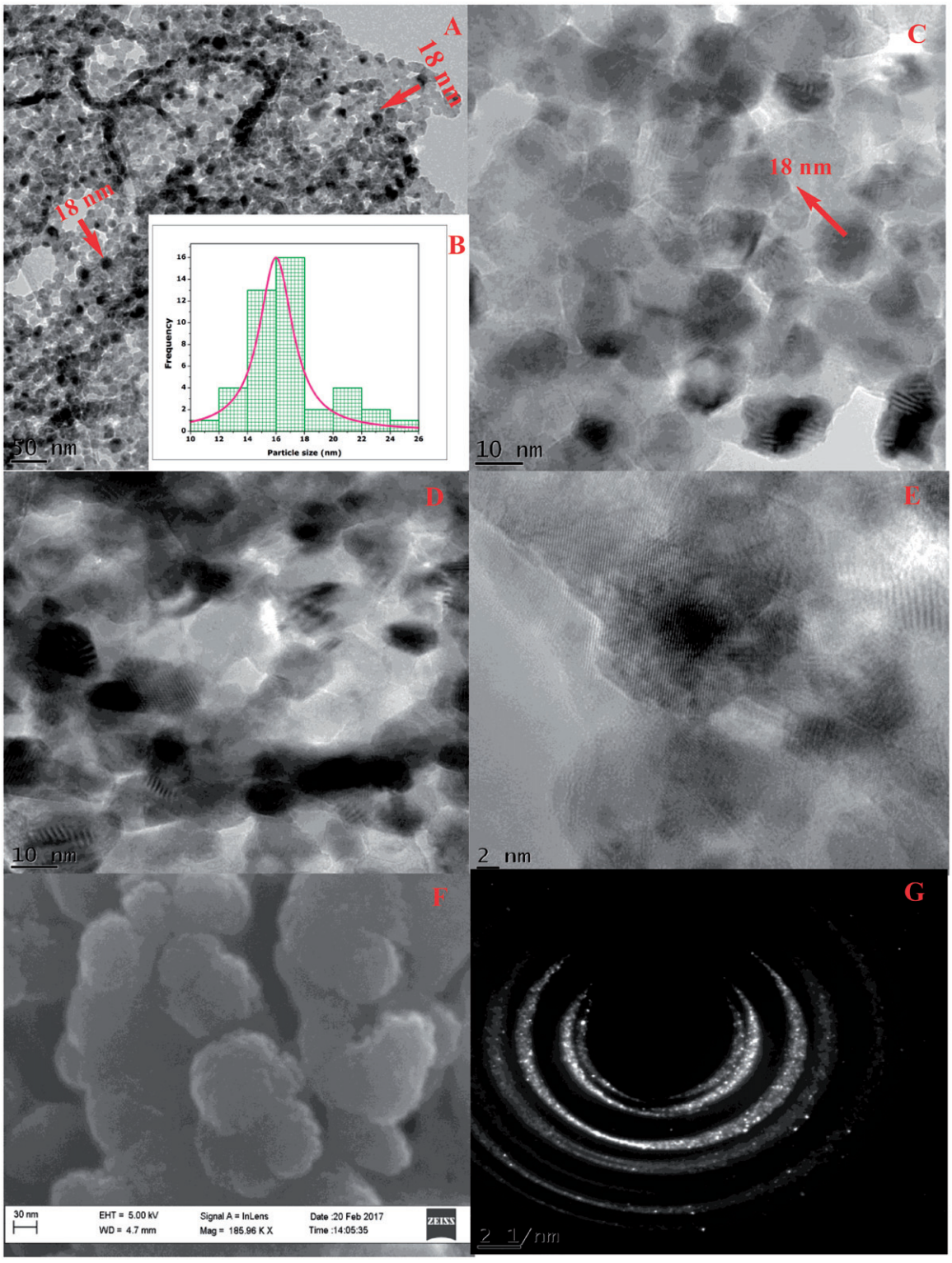

Figure 3. Morphological investigations using HR-TEM/HR-SEM; (A/B/C/D): size distribution of NiO nanoparticles; (E): HR-TEM image; (F): HR-SEM; (G): SAED pattern.

absorption band observed nearly at 3300 cm^{-1} can be attributed to the adhered –OH functional groups. The FTIR spectrum was consistent with XRD results as no impurities are indicated. To further confirm nickel oxide nanoparticles, Raman spectrum was recorded in the spectral range of 0 cm^{-1} to 2000 cm^{-1} as indicated in Figure 4(B). Generally, Raman spectra from NiO have contributions from one phonon LO and TO modes, two phonon excitation and one, two and four magnon excitations. In a case where NiO is anti-ferromagnetically ordered or defect rich, then a significant increase in one phonon scattering [8]. Various characteristic Raman peaks can be observed positioned at ~390 cm^{-1} (1 P), ~652 cm^{-1} (2 P), ~771 cm^{-1} (2 P), ~1064 cm^{-1} (2 P) and ~1660 cm^{-1} (2 M). These peaks are consistent with the earlier reported Raman spectra [38]. Figure 5 presents the EDS spectra to investigate the elemental components of the sample.

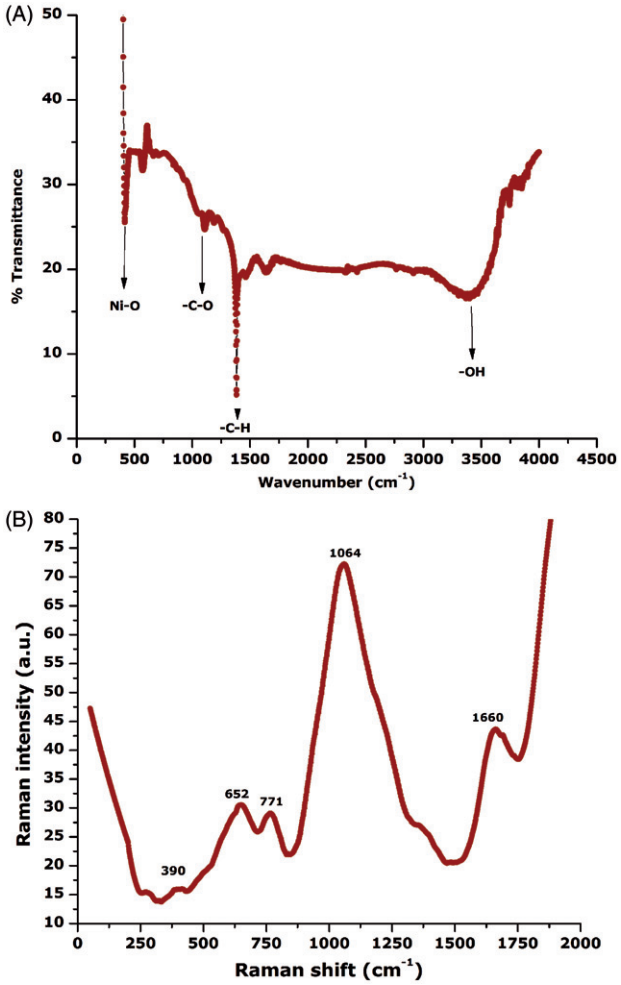

Figure 4. (A) Typical ATR-FTIR of NiO nanoparticles; (B) their Raman spectra.

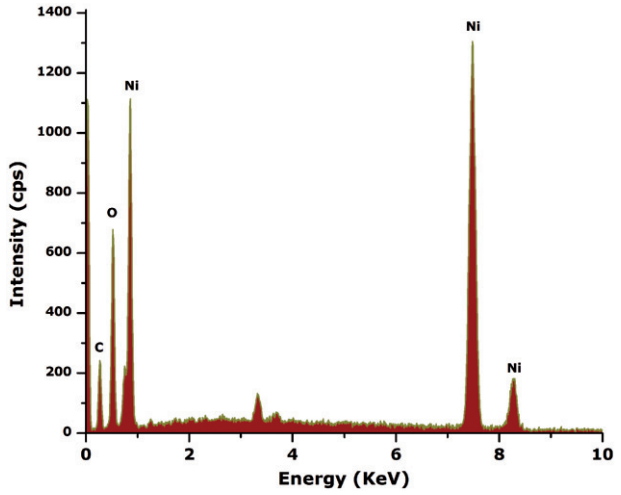

Figure 5. Elemental composition using energy-dispersive spectroscopy (EDS).

Energy-dispersive spectroscopy was carried out for the elemental analysis. Peaks from "Ni" and "O" are evident confirming Ni-O in the sample, while peak indicating "C" is attributed to the grid support.

To check the stability of the colloidal suspension of biosynthesized NiO nanoparticles, 10 mg of NiO nanoparticles were added to 10 ml DMSO and sonicated (Elmasonic) for 15 min. The slightly turbid colloidal suspension was allowed

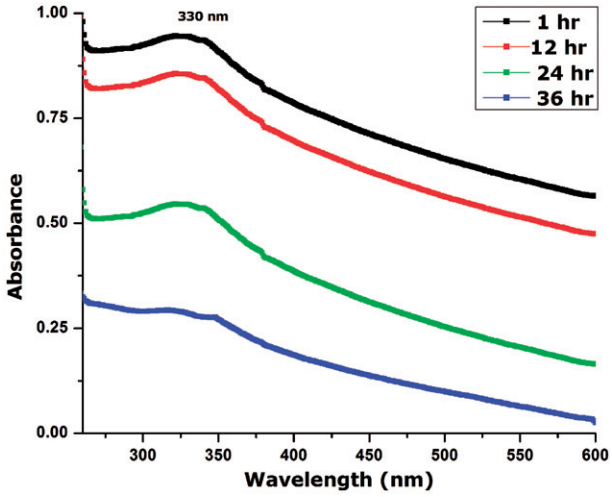

Figure 6. Stability of NiO nanoparticles.

to stand for 48 h and their surface plasmon resonance was monitored using UV spectrophotometer. Stable absorption at ~330 nm indicated that the colloidal suspension was stable for atheist 24 h. The absorption peak is reduced after 24 h, which indicate the settlement of the particles at the bottom of the test tube. The results are indicated in Figure 6.

Antimicrobial activities

Biogenically synthesized nickel oxide nanoparticles were evaluated against 6 pathogenic bacterial strains with and without UV illumination (20 min). Figure 7(A) presents antibacterial activity across the concentration range of 1000 μg/ml–31.25 μg/ml. *Bacillus subtilis* and *E. coli* were found to be the most susceptible strains with zones of inhibition 15.1 mm and 14.1 mm. Only *B. subtilis* was inhibited across all the tested concentrations. MIC was found to be 15.6 μg/ml using broth dilution method. *K. pneumonia* and *P. aeruginosa* were found to be the least susceptible bacterial strains as they were not inhibited at concentrations <250 μg/ml, which was considered as their MIC. Figure 7(B) indicates the antibacterial effect of the bioinspired nickel oxide nanoparticles after UV exposure. Increase is observed in the antibacterial effect after been exposed to the UV. All the bacterial strains were inhibited across all of the used concentrations with only exception of *K. pneumonia* which was not inhibited at concentrations lower than 31.25 μg/ml. *E. coli* and *B. subtilis* were found to be the most susceptible strains with MICs 15.6 μg/ml each. Here, it is noteworthy to mention the use of broth dilution assay to investigate MICs for the concentrations found effective up till 31.25 μg/ml. The results are summarized in Figure 7(A,B) and Table 1. Pure gentamycin 10 μg disc was used as positive control. None of the used samples indicated higher zone of inhibition then the positive control.

Antifungal activities for bioinspired nickel oxide nanoparticles have been rarely investigated. Antifungal activities were performed against 5 pathogenic fungal strains across different concentrations 2 mg/ml to 0.5 mg/ml with Amphotericin B as positive control. All strains were inhibited across the tested concentration indicated NiO as a potential antifungal agent. *M. racemosus* and *R. solani* were found to be most

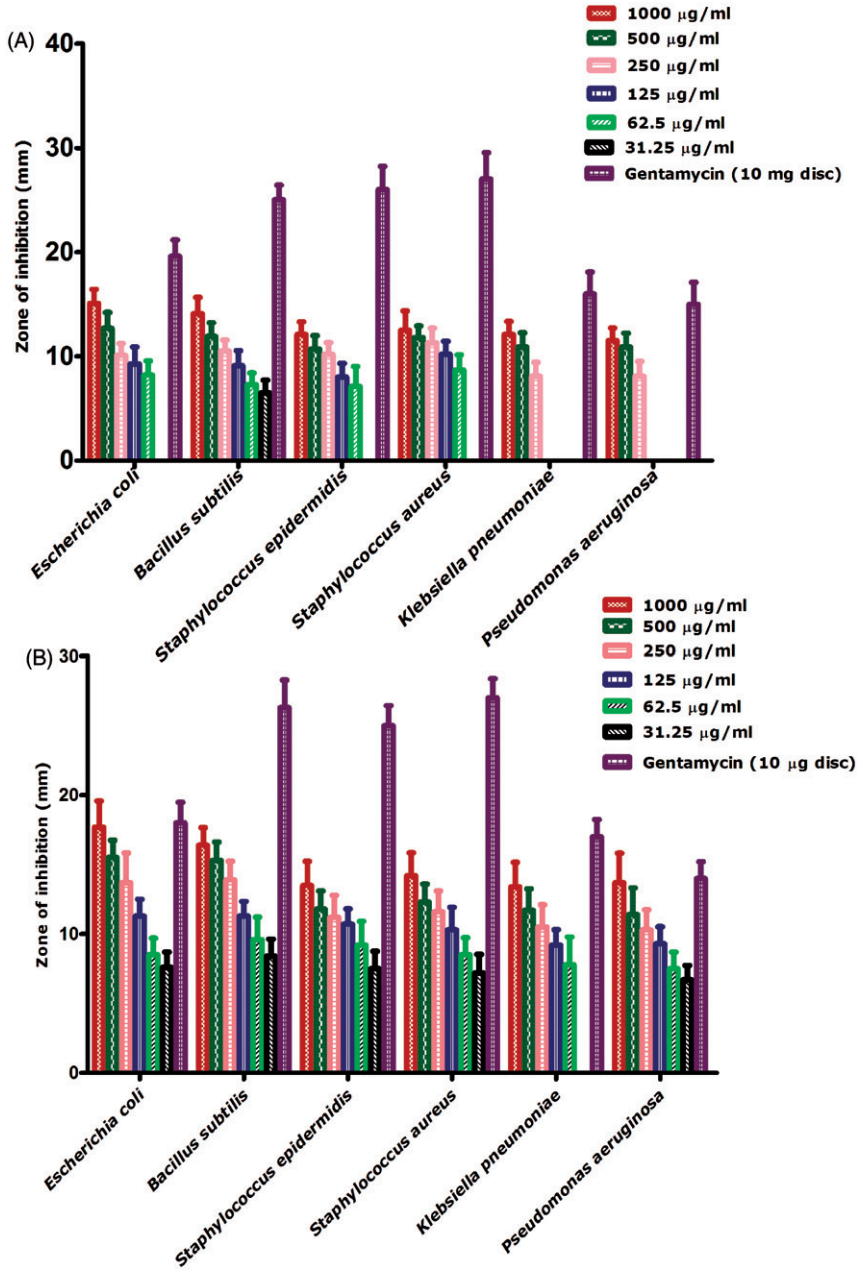

Figure 7. (A) Antibacterial activities of NiO nanoparticles without UV illumination; (B) with UV illumination.

Table 1. MIC calculations against gram positive and gram negative bacterial strains.

Without UV illumination		With UV illumination	
Gram positive		Gram positive	
Bacterial strain	MIC (µg/ml)	Bacterial strain	MIC (µg/ml)
Staphylococcus aureus	62.5	*Staphylococcus aureus*	15.6
Staphylococcus epidermis	62.5	*Staphylococcus epidermis*	7.8
Bacillus subtilis	15.6	*Bacillus subtilis*	7.8
Gram negative		Gram negative	
Klebsiella pneumonia	250	*Klebsiella pneumonia*	62.5
Pseudomonas aeruginosa	250	*Pseudomonas aeruginosa*	15.6
Escherichia coli	62.5	*Escherichia coli*	15.6

susceptible indicated by their percentage inhibition of 64% and 63.2% at 2 mg/ml, respectively. *A. flavus* was indicated as the least susceptible fungal strain. Nanoscale nickel oxide can easily penetrate inside the fungal cells subsequently leading to cellular disruption. Antifungal activities of the as synthesized NiO nanoparticles are presented in Figure 8.

Antileishmanial activity (promastigotes and amastigotes)

Leishmaniasis is a neglected tropical disease and categorized as class 1 disease which is emerging and uncontrolled. Leishmaniasis is an endemic to 98 countries and to date, have no effective vaccines or treatments. ~350 million people are living under the immediate threat of leishmaniasis [39,40]. Current medications are accompanied by certain disadvantages like cost, side effects, elevated toxicity and long duration of therapy. The gold standard treatments include antimonial drugs however they have lost their efficacy due to drug resistance [40]. Leishmania exists in promastigote

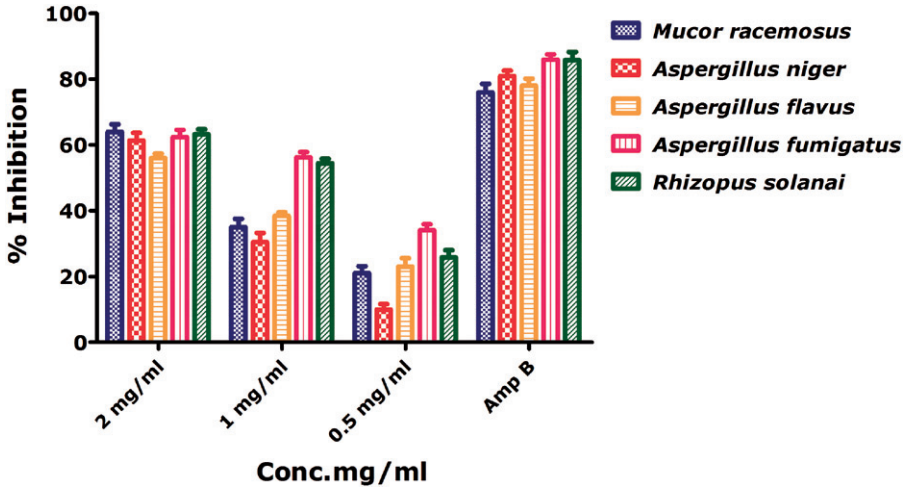

Figure 8. Antifungal potential of bioinspired NiO nanoparticles.

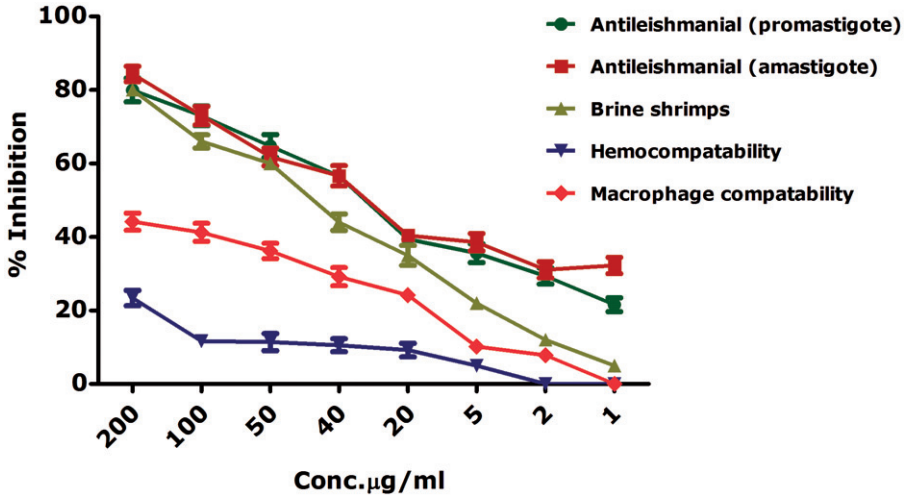

Figure 9. Assessment of the cytotoxicity of the bioinspired NiO nanoparticles.

(motile) form outside the body while transform into amastigote (non-motile) form inside the body. Figure 9 reports the antileishmanial activities of the biosynthesized nickel oxide nanoparticles against the axenic promastigote and amastigote cultures of *Leishmania tropica* using MTT cytotoxic assay. Both cultures were found to be effectively inhibited in a dose-dependent manner. Our results indicate median lethal concentration (IC_{50}) of 24.13 µg/ml and 26.74 µg/ml against leishmania promastigotes and amastigotes, respectively. Amp B indicated IC_{50} values of 1.3 µg/ml and 2.2 µg/ml against the leishmania promastigotes and amastigotes, respectively. Novel strategies by involving nanoparticles for antileishmanial therapy have been a keen area of research. Recently, ZnO [33,41] nanoparticles and silver-doped zinc oxide nanoparticles [42] revealed significant cytotoxic effects against leishmania. It is noteworthy to mention that we have described the antileishmanial potential of bioinspired nickel oxide nanoparticles for the first time. Obtained results also indicated that the NiO nanoparticles were equally effective against the promastigote and amastigote cultures and hence could be used in antileishmanial therapies.

Brine shrimp cytotoxicity

In order to further confirm the cytotoxicity of bioinspired nickel oxide nanoparticles, brine shrimp cytotoxic assay was carried out while their percent mortalities were calculated as indicated in Figure 9. IC_{50} value was calculated as 42.60 µg/ml. *A. salina* is considered as an ideal organism for investigating the cytotoxic potential of a compound [33]. Doxorubicin which was used as a positive control indicated IC_{50} value 3.62 µg/ml. Our results conclude a dose-dependent cytotoxic behavior of the bioinspired zinc oxide nanoparticles. A detailed schematic of the cytotoxicity mechanism is indicated in Figure 10. The IC_{50} values are summarized in Table 2.

Biocompatibility testing

In response to the potential cytotoxic behavior of the as synthesized nickel oxide nanoparticles, their cytotoxicity against the normal human red blood cells and macrophages were assessed. Results are indicated in Figure 9. Results were analyzed over the concentration range from 200 µg/ml to

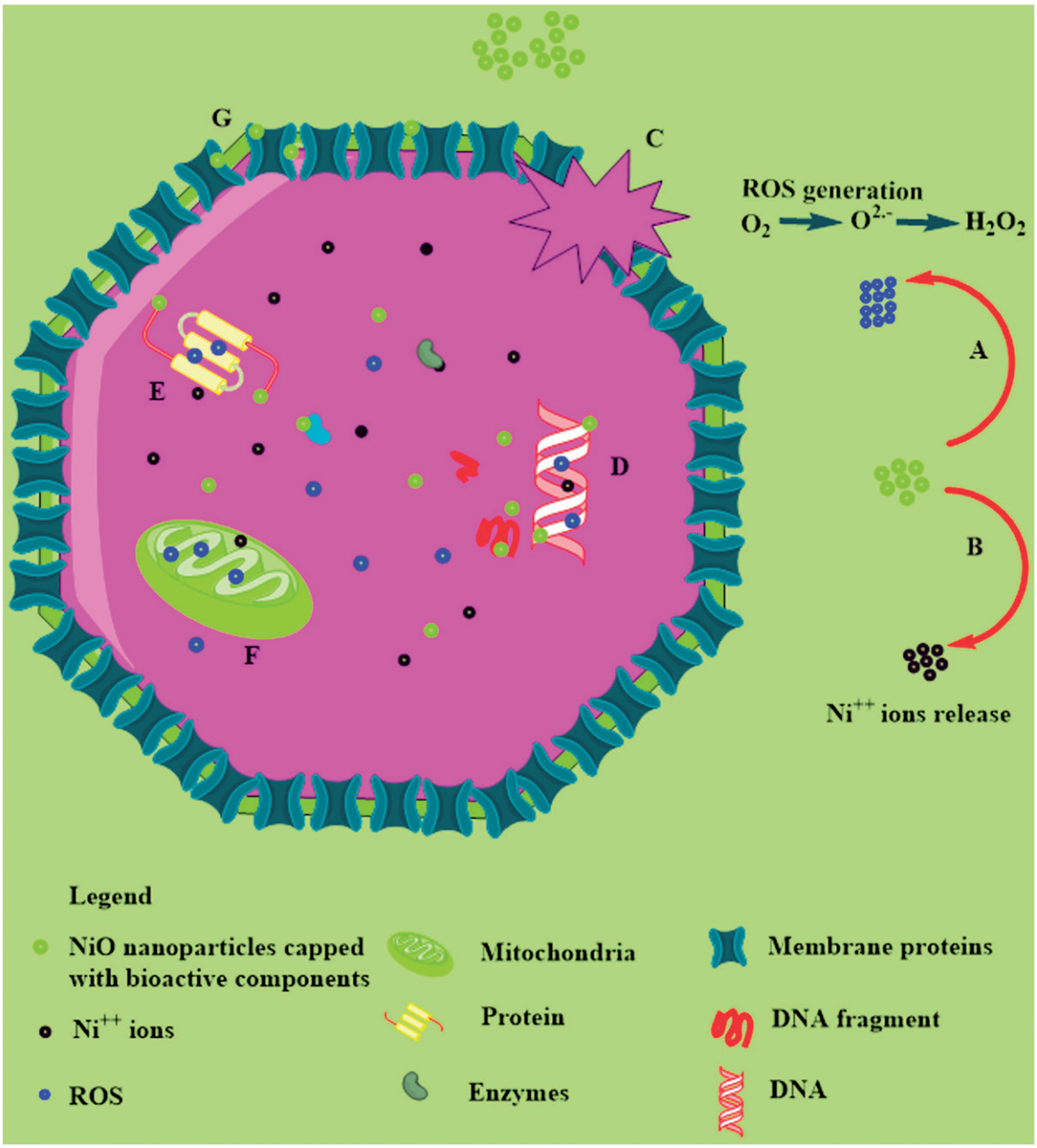

Figure 10. Schematic representation of the cytotoxic properties of bioinspired NiO as reported in literature; (A): ROS generation; (B): Ni^{++} release from NiO; (C): membrane damage by interference of membrane proteins with ROS or with their interference with surface defected NiO; (D): interference of NiO nanoparticles/ROS/Ni^{++} with nuclear material; (E): their interference with proteins; (F): entrance to mitochondrial to generate further ROS; (G): adherence to the membranes and pores.

Table 2. IC_{50} calculations using table curve software.

Assay type	IC_{50}
Antileishmanial promastigotes	24.13 μg/ml
Antileishmanial amastigotes	26.74 μg/ml
Brine shrimp cytotoxicity	42.60 μg/ml
Human RBCs	>200 μg/ml
Human macrophages	>200 μg/ml
Alpha amylase inhibition	>200 μg/ml

1 μg/ml. The hemolytic assay revealed significantly less cytotoxic nature of nickel oxide nanoparticles to the freshly isolated RBCs. Highest hemolysis (23.3%) was observed at the highest dose (200 μg/ml), while no hemolysis was observed at concentrations <5 μg/ml. As compared to the RBCs, macrophages were found more effected with percent mortality of

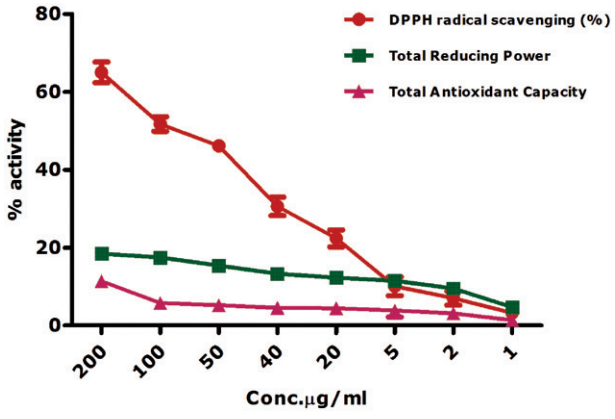

Figure 11. Antioxidant activities of bioinspired NiO.

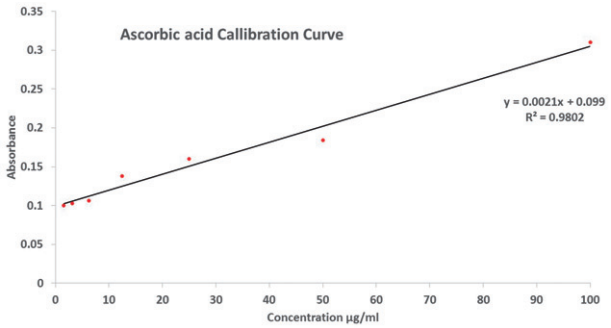

Figure 12. Ascorbic acid calibration curve.

44% at 200 µg/ml. The IC_{50} values were investigated to be >200 µg/ml for the bioinspired nickel oxide nanoparticles against RBCs and macrophages. In general, the test samples can be categorized as safe at low levels. 0.5% Triton X-100 which was used as positive control indicated 73% hemolysis.

Antioxidant activities

Biogenically synthesized nickel oxide nanoparticles were found to have DPPH radical scavenging ability 65% to 3.27% across all the tested concentrations ranging from 200 µg/ml to 1 µg/ml. DPPH has been widely used as a gold standard to investigate the free radical scavenging activity of NiO nanoparticles, however to date bioinspired nickel oxide nanoparticles have not been investigated for free radical scavenging. Previous researchers have considered chemically synthesized nickel oxide nanoparticles as novel antioxidant because of their free radical scavenging potential [43]. The role of defects in the free radical scavenging ability of chemically synthesized nano-nickel oxide is also established [43,44]. This study also confirms free radical scavenging potential for the bioinspired nickel oxide nanoparticles. The antioxidant potency of was due to the quenching ability of the DPPH-free radical in a concentration-dependent manner.

DPPH-free radical scavenging by nanoscale nickel oxide was also supported by the total antioxidant capacity using ferric ions as a chelating agent. Antioxidant capacity was expressed in as total ascorbic acid equivalents (µg) per mg. At 200 µg/ml, 11.3 µg AAE/mg were recorded. Oxidation is a natural process occurring in living cells can lead to the generation of ROS, which can interfere to de-normalize the cellular physiology. Insufficient availability of antioxidants can have dreadful results like lipid peroxidation, enzyme inactivation, protein and DNA damage. Further assessment of the antioxidant potential of the bioinspired NiO nanoparticles was carried out via studying their reducing power potential. Reducing power potential decreased with the lowering of test sample concentration. Overall, a good DPPH-free radical scavenging and moderate antioxidant capacity and reducing power can be concluded for the bioinspired nano-nickel oxide. The results of the antioxidant activities are presented in Figure 11.

Ascorbic acid calibration curve in the range of 0–1000 µg/ml was used to calculate the equivalents amounts of ascorbic acid in the sample using trend-line. The standard curve of the ascorbic acid is indicated in Figure 12.

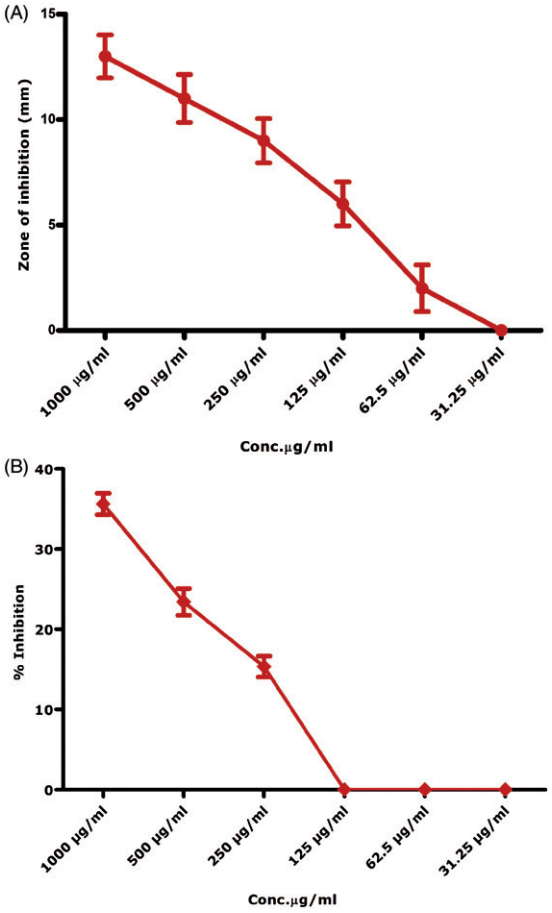

Figure 13. (A): Protein kinase inhibition potential; (B): alpha amylase inhibition potential.

Enzyme inhibition assays

Figure 13(A) presents the protein kinase enzyme inhibition potential of the biogenic nickel oxide nanoparticles. Protein kinase enzymes are considered as a crucial area for anticancer research. PK enzymes are responsible for the phosphorylation of serine–threonine and tyrosine amino acid residues that play role in the cellular differentiation, proliferation and apoptosis. Cancer is associated with the deregulated phosphorylation by PK enzymes leading to tumor growth. Therefore, particular entities which can inhibit PK enzymes are of significant interest in anticancer research. PK phosphorylation is a key factor in the formation of hyphae in *Streptomyces* and therefore has been extensively used to identify PK inhibitors. *Streptomyces* 85E strain was used to screen PK inhibition potential of the as synthesized NiO nanoparticles. Bald zones were measured in mm. Largest zone (13 mm) was recorded at 1000 µg/ml. All tested concentration produced bald zones except for 31.25 µg/ml which was found to be effective. Our results indicate that biomodulated NiO can be used as a signal transductor inhibitor in the genesis of tumor. Surfactin employed as a positive control which yielded higher zone of

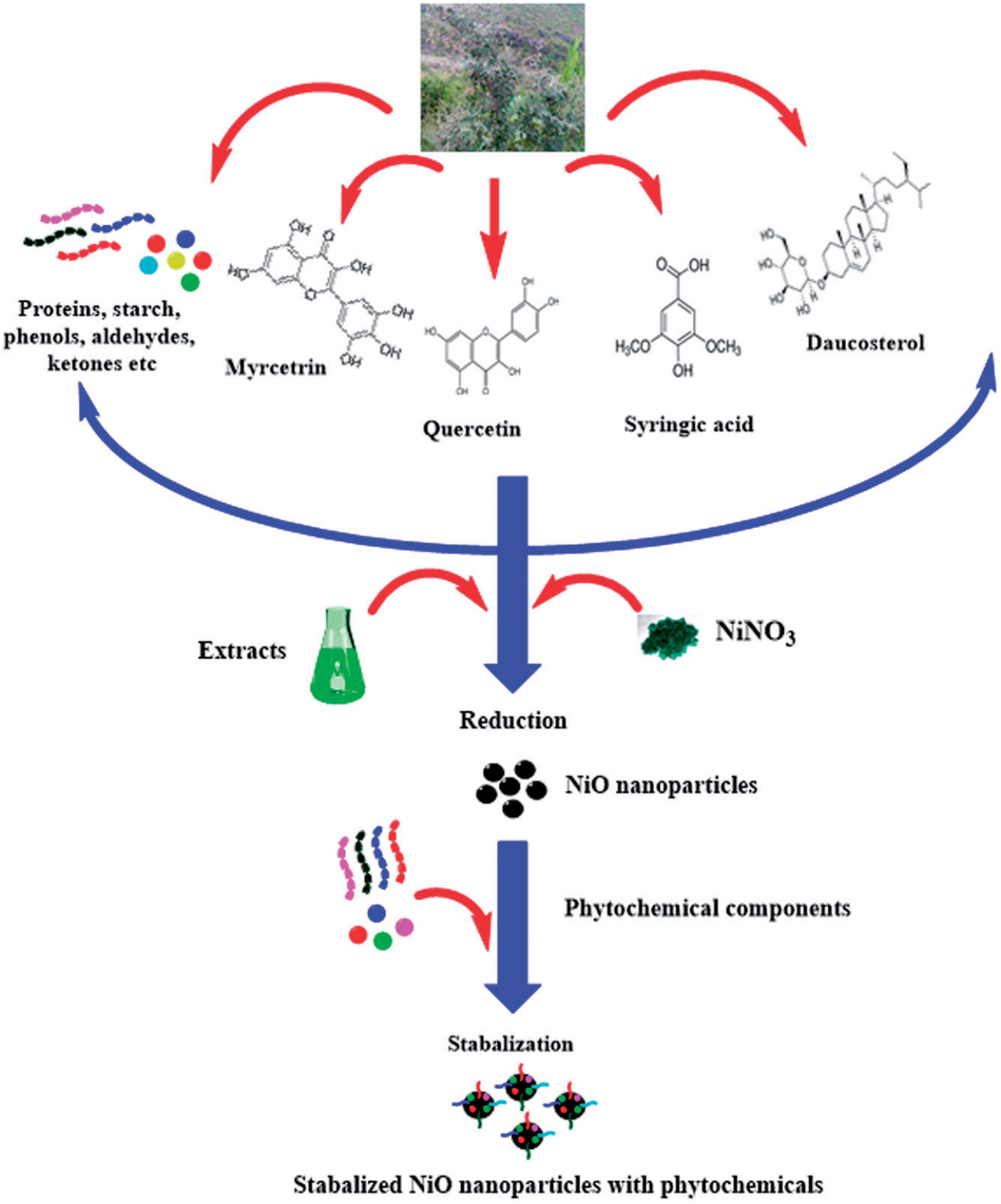

Figure 14. Plausible mechanism for the biosynthesis of NiO nanoparticles via green route.

inhibition, that is, 18 mm at 1000 μg/ml and 7.4 mm at 31.25 μg/ml.

Figure 13(B) indicates the alpha amylase enzyme inhibition potential of the biogenically synthesized NiO nanoparticles. This enzyme catalyzes carbohydrate breakdown to glucose and therefore has been related to the postprandial glucose excursion in a patient suffering from diabetes. Hence, alpha amylase enzyme inhibitors have been considered in diabetes research. Our results indicate that low alpha amylase enzyme inhibition (35%) at higher concentrations as high as 1000 μg/ml, whereas the bioinspired nickel oxide was found to be ineffective at lower concentrations

<250 μg/ml. On the other hand, acarbose (1 μM) was used as a standard alpha amylase inhibitor and yielded a percentage inhibition of 92%.

Discussion

A green route for the biosynthesis of NiO nanoparticles has been revealed using the aqueous leaf extracts of *S. thea*. Biomimetic synthesis of nanoparticles is considered more acceptable and eco-friendly [17,45–52]. *Sageretia thea* has well-documented medicinal uses and been used as tea in parts of Korea and China. Various compound like Syringic acid, Taraxerol, Quercetin, Kaempferol, Myricetrin and Daucosterol, etc. [53–55] have been isolated which can play a role in reduction and stabilization in the biosynthesis of nanoparticles. A plausible mechanism for the biosynthesis is indicated in Figure 14. Mostly phenolic and flavonoid compounds are involved in the biosynthesis of nanoparticles, however, the exact mechanism by which nanoparticles are produced is an open area of research. Successful green synthesis of NiO nanoparticles using plants has also been previously reported by various researchers [2,8,17,29]. Single and pure phase of NiO nanoparticles were successfully demonstrated through characterization techniques. Good antibacterial potential can be concluded for the as synthesized NiO nanoparticles. In general, gram positive bacterial strains were found to be more susceptible which is in good agreement with the previous studies [2,56]. UV illumination increased the antibacterial activity of nanoparticles. The role of UV illumination in enhancement of the ROS generation has been previously established which is considered as the mechanism for bacterial growth inhibition [57]. The precise antibacterial mechanism against particular type of bacteria is however debatable. Proposed electrostatic interactions between the negatively charged bacterial cell membrane and positively charged nickel ions (Ni^{++}), released from the nickel oxide nanoparticles may penetrate inside the cell wherein it interferes with cellular physiology leading to their disruption. NiO can also alter the membrane permeability leading to protein leakage [58,59] Enhancement of the antibacterial activity after UV illumination could be the generation of holes (h^{+}) and electrons (e^{-}) which has higher oxidizing and reducing abilities. Hence, they may react subsequently with water, hydroxyl ions and oxygen to yield further reactive oxygen species like $H_2O_2^{\bullet}$, $O^{2\bullet-}$ and •OH, that possess a significant tendency to destroy the cells by interfering with proteins, DNA, mitochondria and other cellular components [60,61]. *Sageretia thea* aqueous leaf extracts were found capable for producing small size nanoparticles ∼18 nm. Size is a crucial factor in the antimicrobial properties of nanoparticles [62,63]. Smaller size is associated with enhanced antimicrobial nature. Cytotoxic nature of bioinspired NiO nanoparticles has been indicated in recent reports which are in agreement to our findings [2]. The cytotoxic nature of bioinspired nanoparticles was confirmed against Leishmania promastigotes, amastigotes and brine shrimps. Moderate antioxidant and enzyme inhibition activities are reported.

Biogenic nickel oxide nanoparticles have been rarely investigated for biological properties. To the best of our knowledge, this current report is the first report on the antioxidant, enzyme inhibition and antileishmanial potential of the biogenic nickel oxide nanoparticles.

Conclusions

Nanoscale nickel oxide was biologically synthesized using aqueous leaf extracts of medicinally important plant *S. thea*, and their *in vitro* antimicrobial, cytotoxic, biocompatibility, antioxidant and enzyme inhibition properties were revealed. Bioinspired nickel oxide nanoparticles indicated enhancement in the antibacterial activities after UV illumination, while they were found to be effective against pathogenic fungal strains. Significant antileishmanial potential and moderate antioxidant potential is revealed by the bioinspired NiO nanoparticles. Furthermore, moderate enzyme inhibition activities are also reported. Bioinspired NiO was found to be less toxic to normal human blood cells like RBCs and macrophages. Overall, we conclude bioinspired nickel oxide nanoparticles as a potential candidate for biomedical applications because of their interesting properties. We recommend further studies on the drug delivery and effect of UV on the biological properties of NiO nanoparticles.

Acknowledgements

This research was supported by National Research Foundation (NRF) and UNESO-UNISA Africa Chair in nanoscience and nanotechnology. The authors are indebted to the fellows at Material Research Department, iThemba Labs, for their continuous humble support and cooperation. The authors acknowledge the support of Prof. NM Butt from Preston University. Mr. Ali Talha Khalil is also affiliated with Department of Biotechnology, Quaid-i-Azam University, Islamabad, Pakistan.

Disclosure statement

No potential conflict of interest was reported by the authors.

Funding

This research was supported by National Research Foundation (NRF) and UNESO-UNISA Africa Chair in nanoscience and nanotechnology.

References

[1] Hao R, Xing R, Xu Z, et al. Synthesis, functionalization, and biomedical applications of multifunctional magnetic nanoparticles. Adv Mater. 2010;22:2729–2742.

[2] Ezhilarasi AA, Vijaya JJ, Kaviyarasu K, et al. Green synthesis of NiO nanoparticles using *Moringa oleifera* extract and their biomedical applications: cytotoxicity effect of nanoparticles against HT-29 cancer cells. J Photochem Photobiol B Biol. 2016;164:352–360.

[3] Lokesh K, Kavitha G, Manikandan E, et al. Effective ammonia detection using n-ZnO/p-NiO heterostructured nanofibers. IEEE Sens J. 2016;16:2477–2483.

[4] Manikandan E, Kennedy J, Kavitha G, et al. Hybrid nanostructured thin-films by PLD for enhanced field emission performance for radiation micro-nano dosimetry applications. J Alloys Comp. 2015;647:141–145.

[5] Brigger I, Dubernet C, Couvreur P. Nanoparticles in cancer therapy and diagnosis. Adv Drug Deliv Rev. 2002;54:631–651.
[6] Whitesides GM. Nanoscience, nanotechnology, and chemistry. Small. 2005;1:172–179.
[7] Sasi B, Gopchandran K, Manoj P, et al. Preparation of transparent and semiconducting NiO films. Vacuum. 2002;68:149–154.
[8] Sone B, Fuku X, Maaza M. Physical and electrochemical properties of green synthesized Bunsenite NiO nanoparticles via *Callistemon viminalis*' extracts. Int J Electrochem Sci. 2016;11:8204–8220.
[9] Pandian CJ, Palanivel R, Dhananasekaran S. Green synthesis of nickel nanoparticles using *Ocimum sanctum* and their application in dye and pollutant adsorption. Chinese J Chem Eng. 2015; 23:1307–1315.
[10] Sudhasree S, Shakila Banu A, Brindha P, et al. Synthesis of nickel nanoparticles by chemical and green route and their comparison in respect to biological effect and toxicity. Toxicol Environ Chem. 2014;96:743–754.
[11] Gong N, Shao K, Feng W, et al. Biotoxicity of nickel oxide nanoparticles and bio-remediation by microalgae *Chlorella vulgaris*. Chemosphere. 2011;83:510–516.
[12] Zhang Y. Thermal oxidation fabrication of NiO film for optoelectronic devices. Appl Surf Sci. 2015;344:33–37.
[13] Kundu M, Liu L. Binder-free electrodes consisting of porous NiO nanofibers directly electrospun on nickel foam for high-rate supercapacitors. Mater Lett. 2015;144:114–118.
[14] Ksapabutr B, Nimnuan P, Panapoy M. Dense and uniform NiO thin films fabricated by one-step electrostatic spray deposition. Mater Lett. 2015;153:24–28.
[15] Soomro RA, Ibupoto ZH, Abro MI, et al. Electrochemical sensing of glucose based on novel hedgehog-like NiO nanostructures. Sens Actuat Chem. 2015;209:966–974.
[16] Tao K, Li P, Kang L, et al. Facile and low-cost combustion-synthesized amorphous mesoporous NiO/carbon as high mass-loading pseudocapacitor materials. J Power Sources. 2015;293:23–32.
[17] Thema F, Manikandan E, Gurib-Fakim A, et al. Single phase Bunsenite NiO nanoparticles green synthesis by *Agathosma betulina* natural extract. J Alloys Comp. 2016;657:655–661.
[18] Thovhogi N, Diallo A, Gurib-Fakim A, et al. Nanoparticles green synthesis by *Hibiscus sabdariffa* flower extract: main physical properties. J Alloys Comp. 2015;647:392–396.
[19] Thema F, Manikandan E, Dhlamini M, et al. Green synthesis of ZnO nanoparticles via *Agathosma betulina* natural extract. Mater Lett. 2015;161:124–127.
[20] Thema F, Beukes P, Gurib-Fakim A, et al. Green synthesis of Monteponite CdO nanoparticles by *Agathosma betulina* natural extract. J Alloys Comp. 2015;646:1043–1048.
[21] Ovais M, Khalil AT, Raza A, et al. Green synthesis of silver nanoparticles via plant extracts: beginning a new era in cancer theranostics. Nanomedicine. 2016;12:3157–3177.
[22] Kar A, Ray AK. Synthesis of nano-spherical nickel by templating hibiscus flower petals. NANO. 2014;2:17–20.
[23] Khan I, AbdElsalam NM, Fouad H, et al. Application of ethnobotanical indices on the use of traditional medicines against common diseases. Evid Based Complement Altern Med. 2014;2014. http://dx.doi.org/10.1155/2014/635371
[24] Hyun TK, Song SC, Song C-K, et al. Nutritional and nutraceutical characteristics of *Sageretia theezans* fruit. J Food Drug Anal. 2015;23:742–749.
[25] Murad W, Ahmad A, Gilani SA, et al. Indigenous knowledge and folk use of medicinal plants by the tribal communities of Hazar Nao Forest, Malakand District, North Pakistan. J Med Plants Res. 2011;5:1072–1086.
[26] Salvadori MR, Ando RA, Nascimento CAO, et al. Extra and intracellular synthesis of nickel oxide nanoparticles mediated by dead fungal biomass. PLoS One. 2015;10:e0129799.
[27] Salvadori MR, Nascimento CAO, Corrêa B. Nickel oxide nanoparticles film produced by dead biomass of filamentous fungus. Sci Rep. 2014;4:6404.
[28] Yuvakkumar R, Suresh J, Nathanael AJ, et al. Rambutan (*Nephelium lappaceum* L.) peel extract assisted biomimetic synthesis of nickel oxide nanocrystals. Mater Lett. 2014;128:170–174.
[29] Nasseri M, Ahrari F, Zakerinasab B. A green biosynthesis of NiO nanoparticles using aqueous extract of *Tamarix serotina* and their characterization and application. Appl Organometal Chem. 2016;30:978–984.
[30] Fatima H, Khan K, Zia M, et al. Extraction optimization of medicinally important metabolites from Datura innoxia Mill.: an in vitro biological and phytochemical investigation. BMC Complement Altern Med. 2015;15:376.
[31] Ahmad K, talha Khalil A, Somayya R. Antifungal, phytotoxic and hemagglutination activity of methanolic extracts of *Ocimum basilicum*. J Trad Chinese Med. 2016;36:794–798.
[32] Khan I, Ahmad K, Khalil AT, et al. Evaluation of antileishmanial, antibacterial and brine shrimp cytotoxic potential of crude methanolic extract of herb *Ocimum basilicum* (Lamiacea). J Trad Chinese Med. 2015;35:316–322.
[33] Ali A, Ambreen S, Javed R, et al. ZnO nanostructure fabrication in different solvents transforms physio-chemical, biological and photodegradable properties. Mater Sci Eng C. 2017;74:137–145.
[34] Chtita S, Ghamali M, Hmamouchi R, et al. Investigation of antileishmanial activities of acridines derivatives against promastigotes and amastigotes form of parasites using quantitative structure activity relationship analysis. Adv Phys Chem. 2016;2016. http://dx.doi.org/10.1155/2016/5137289
[35] Malagoli D. A full-length protocol to test hemolytic activity of palytoxin on human erythrocytes. Inverteb Surv J. 2007;4:92–94.
[36] Jafri L, Saleem S, Ullah N, Mirza B. In vitro assessment of antioxidant potential and determination of polyphenolic compounds of *Hedera nepalensis* K. Koch. Arab J Chem. 2014;10:S3699–S3706.
[37] Javed R, Usman M, Tabassum S, et al. Effect of capping agents: structural, optical and biological properties of ZnO nanoparticles. Appl Surf Sci. 2016;386:319–326.
[38] Mironova-Ulmane N, Kuzmin A, Steins I, et al. Raman scattering in nanosized nickel oxide NiO. J Phys Conf Ser. 2007;93:012039.
[39] Abamor ES. Antileishmanial activities of caffeic acid phenethyl ester loaded PLGA nanoparticles against *Leishmania infantum* promastigotes and amastigotes in vitro. Asian Pacific J Trop Med. 2017;10:25–34.
[40] Légaré D, Ouellette M. Drug resistance in Leishmania. Handbook of antimicrobial resistance. New York (NY): Springer, 2017. pp. 313–341.
[41] Nadhman A, Khan MI, Nazir S, et al. Annihilation of Leishmania by daylight responsive ZnO nanoparticles: a temporal relationship of reactive oxygen species-induced lipid and protein oxidation. Int J Nanomedicine. 2016;11:2451.
[42] Nadhman A, Sirajuddin M, Nazir S, et al. Photo-induced Leishmania DNA degradation by silver-doped zinc oxide nanoparticle: an in-vitro approach. IET Nanobiotechnol. 2016;10:129–133.
[43] Saikia JP, Paul S, Konwar BK, et al. Nickel oxide nanoparticles: a novel antioxidant. Colloids Surf B Biointerfaces. 2010;78:146–148.
[44] Madhu G, Bose VC, Aiswaryaraj A, et al. Defect dependent antioxidant activity of nanostructured nickel oxide synthesized through a novel chemical method. Colloids Surf A Physicochem Eng Asp. 2013;429:44–50.
[45] Diallo A, Ngom B, Park E, et al. Green synthesis of ZnO nanoparticles by *Aspalathus linearis*: structural and optical properties. J Alloys Comp. 2015;646:425–430.
[46] Sone B, Manikandan E, Gurib-Fakim A, et al. Sm_2O_3 nanoparticles green synthesis via *Callistemon viminalis*' extract. J Alloys Comp. 2015;650:357–362.
[47] Thovhogi N, Park E, Manikandan E, et al. Physical properties of CdO nanoparticles synthesized by green chemistry via *Hibiscus sabdariffa* flower extract. J Alloys Comp. 2016;655:314–320.
[48] Diallo A, Manikandan E, Rajendran V, et al. Physical & enhanced photocatalytic properties of green synthesized SnO_2 nanoparticles via *Aspalathus linearis*. J Alloys Comp. 2016;681:561–570.

[49] Sone B, Manikandan E, Gurib-Fakim A, et al. Single-phase α-Cr2O3 nanoparticles' green synthesis using *Callistemon viminalis*' red flower extract. Green Chem Lett Rev. 2016;9:85–90.
[50] Diallo A, Beye A, Doyle T, et al. Green synthesis of Co3O4 nanoparticles via *Aspalathus linearis*: physical properties. Green Chem Lett Rev. 2015;8:30–36.
[51] Khenfouch M, Minnis Ndimba R, Diallo A, et al. *Artemisia herba-alba Asso* eco-friendly reduced few-layered graphene oxide nanosheets: structural investigations and physical properties. Green Chem Lett Rev. 2016;9:122–131.
[52] Venugopal K, Rather H, Rajagopal K, et al. Synthesis of silver nanoparticles (AgNPs) for anticancer activities (MCF 7 breast and A549 lung cell lines) of the crude extract of *Syzygium aromaticum*. J Photochem Photobiol B Biol. 2017;167:282–289.
[53] Shen CJ, Chen CK, Lee SS. Polar constituents from *Sageretia thea* leaf characterized by HPLC-SPE-NMR assisted approaches. J Chinese Chem Soc. 2009;56:1002–1009.
[54] Chung S-K, Kim Y-C, Takaya Y, et al. Novel flavonol glycoside, 7-O-methyl mearnsitrin, from *Sageretia theezans* and its antioxidant effect. J Agric Food Chem. 2004;52:4664–4668.
[55] Xu L, Yang X, Li B. Chemical constituents of *Sageretia theezans* Brongn. Zhongguo Zhong yao za zhi. J Chinese Mater Med. 1994;19:675–676.
[56] Helen SM, Rani MHE. Characterization and antimicrobial study of nickel nanoparticles synthesized from dioscorea (Elephant yam) by green route. Int J Sci Res. 2015;4:216–219.
[57] Zhang H, Chen B, Jiang H, et al. A strategy for ZnO nanorod mediated multi-mode cancer treatment. Biomaterials. 2011;32:1906–1914.
[58] Wong KK, Liu X. Silver nanoparticles – the real "silver bullet" in clinical medicine? Med Chem Commun. 2010;1:125–131.
[59] Baek Y-W, An Y-J. Microbial toxicity of metal oxide nanoparticles (CuO, NiO, ZnO, and Sb2O3) to *Escherichia coli*, *Bacillus subtilis*, and *Streptococcus aureus*. Sci Total Environ. 2011;409:1603–1608.
[60] Burello E, Worth AP. A theoretical framework for predicting the oxidative stress potential of oxide nanoparticles. Nanotoxicology. 2011;5:228–235.
[61] Du J, Gebicki JM. Proteins are major initial cell targets of hydroxyl free radicals. Int J Biochem Cell Biol. 2004;36:2334–2343.
[62] Nel A, Xia T, Mädler L, et al. Toxic potential of materials at the nanolevel. Science. 2006;311:622–627.
[63] Jiang W, Mashayekhi H, Xing B. Bacterial toxicity comparison between nano-and micro-scaled oxide particles. Environ Poll. 2009;157:1619–1625.